Mathematical optimisation of laminar forced convection heat transfer through a vascularised solid with square channels

O.T. Olakoyejo, T. Bello-Ochende* and J.P. Meyer

Department of Mechanical and Aeronautical Engineering, University of Pretoria, Pretoria Private Bag X20, Hatfield 0028, South Africa.

Abstract

This paper presents a three-dimensional geometric optimisation of cooling channels in forced convection of a vascularised material with the localised self-cooling property subjected to a heat flux. A square configuration was studied with different porosities. Analytical and numerical solutions were provided. The geometrical configuration was optimised in such a way that the peak temperature was minimised at every point in the solid body. The optimisation was subject to the constraint of a fixed global volume of solid material, but the elemental volume was allowed to morph. The solid material was subject to a heat flux on one side and the cooling fluid was forced through the channels from the opposite direction with a specified pressure difference. The structure had three degrees of freedom as design variables: the elemental volume, channel hydraulic diameter and channel-to-channel spacing. A gradient-based optimisation algorithm was used to determine the optimal geometry that gave the lowest thermal resistance. This optimiser adequately handled the numerical objective function obtained from numerical simulations of the fluid flow and heat transfer. The numerical results obtained were in agreement with a theoretical formulation using scale analysis and the method of intersection of asymptotes. The results obtained show that as the pressure difference increases, the minimised thermal resistance decreases. The results also show the behaviour of the applied pressure difference on the optimised geometry. The use of

* Corresponding author. Tel.: +27 12 4203105; fax: +27 12 362 5124
E-mail address: tuned.bello-ochende@up.ac.za

the optimiser made the numerical results to be more robust with respect to the optimum internal configurations of the flow systems and the dimensionless pressure difference.

Keywords: mathematical optimization, vascularization, constructal theory, square channels, dynamic-Q

Nomenclature

A_c	Cross-sectional area of the channel, m^2
A_s	Cross-sectional area of the structure, m^2
Be	Bejan number
C_P	Specific heat at constant pressure, J/kg K
d_h	Hydraulic diameter, m
H	Structure height, m
h	Elemental height , m
h_c	Channel height , m
i	Mesh iteration index
k	Thermal conductivity, W/mK
L	Axial length, m
N	Number of channels
n	Normal
P	Pressure, Pa
q''	Heat flux, W/m^2
R	Thermal resistance
s	Channel spacing, m
T	Temperature, ^0C

u	Velocity, m/s
$\vec{u}$	Velocity vector, m/s
V	Global structure volume, m^3
v_c	Channel volume, m^3
v_{el}	Elemental volume, m^3
W	Structure width, m
w	Elemental width, m
w_c	Cooling channel width, m
x, y, z	Cartesian coordinates, m

Greek symbols

α	Thermal diffusivity, m^2/s
μ	Viscosity, kg/m.s
ρ	Density, kg/m^3
∂	Differential
∞	Far extreme end, free stream
ϕ	Porosity
Δ	Difference
∇	Differential operator
γ	Convergence criterion

Subscripts

f	Fluid
in	Inlet
max	Maximum, peak
min	Minimum

opt Optimum

r Ratio

s Solid

w Wall

1. Introduction

Material with the property of self-healing and self-cooling is becoming more promising in heat transfer analysis [1-7]. The development of vascularisation of materials indicates flow architectures that conduct and circulate fluids at every point within the solid body. This solid body (slab) may be performing or experiencing mechanical functions such as mechanical loading, sensing and morphing. The self-cooling ability of vascularised material to bathe volumetrically at every point of a solid body gave birth to the name "smart material". Constructal theory and design [8, 9] have been adopted as an optimisation technique for the development of a procedure that is sufficiently allocating and optimising a fixed global space constraint using a physical law (constructal law). The method seeks to optimise the flow architecture that predicts the flow and thermal fluid behaviour in a structure that is subject to a global volume constraint. Bejan [8, 9] stated this law as: *For a finite-size system to persist in time (to live), it must evolve in such a way that it provides easier access to the imposed (global) currents that flow through it*. In a smart material, constructal theory ideally helps in the vascularisation of the smart material structure by morphing the flow architecture configuration to provide easier and greater access of flow through it.

The application of this theory started with Bejan and Sciubba [10], who obtained a dimensionless pressure difference number for optimal spacing from board to board of an array of parallel plates to channel length ratio and a maximum heat transfer density, which can be fitted in a fixed volume in an electronic cooling application using the method of intersection

of asymptotes. The applications of this theory have been reviewed [11, 12] where, under certain global constraints, the best architecture of a flow system can be achieved with the one that gives less global flow resistances, or allows high global flow access. In other words, the shapes of the channels and the elemental structure that is subject to global constraint are allowed to morph. The optimisation of heat exchangers and multiscale devices by constructal theory has also recently been reviewed and summarised by Reis [13] and Fan and Luo [14].

Bello-Ochende *et al*. [15] conducted a three-dimensional optimisation of heat sinks and cooling channels with heat flux using scale analysis and the intersection of asymptotes method based on constructal theory to investigate and predict the design and optimisation of the geometric configurations of the cooling channels. Rocha *et al*. [16] and Biserni *et al*. [17] applied the theory to optimise the geometry of C- and H-shaped cavities respectively that intrude into a solid conducting wall in order to minimise the thermal resistance between the solid and the cavities, Lorenzini *et al.* [18] used the theory to minimise the thermal resistance between the solid and the cavities by optimising the geometry of isothermal cavities that evolve from T- and Y-shaped of a solid conducting wall.

Cho *et al* [19] numerically investigated the flow and thermal behaviour of vascular cooling plate for the volumetric bathing of the smart structures. Constructal theory applications on the vascularisation revolution of smart materials can also be found in open literature [20-25]. Also, the constructal theory for optimisation of several components and systems and components in engineering applications has been extensively discussed and documented in the literature [26-29].

The recent comment by Meyer [30] on the latest review of constructal theory by Bejan and Lorente [31] shows that the application of constructal law in all fields of educational design is a wide road to future advances.

This paper is borne out of the work of Kim *et al.* [7], who theoretically and numerically analysed vascularised materials with heating from one side and coolant forced from the other side for parallel plates and cylindrical channel configurations in an attempt to find the channel configurations that minimised the non-uniform temperature distribution of a vascularised solid body. This paper focuses on the mathematical optimisation of laminar forced convection heat transfer through a vascularised solid with square channels. It examines the optimisation of a fixed and finite global volume of solid material with an array of square cooling channels, with a uniform heat flux from one side. The objective is the building of a smaller construct to form part of a larger construct body with a self-cooling function that will lead to the minimisation of the global thermal resistance or, inversely, the maximisation of the heat transfer rate density (the total heat transfer rate per unit volume). This is achieved by designing the body in a vascularised manner and by forcing a coolant to the heated spot in a fast and efficient way so as to significantly reduce the peak temperature at any point inside the volume that needs cooling. The solution of Kim *et al.* [7] will be used as comparison for the results reported in this paper.

2. Computational model

The schematic diagram of the physical configuration is shown in Figure 1. The system consists of a solid body of fixed global volume, V, which is heated with uniform heat flux q'' on the left side. The body is cooled by forcing a single-phase cooling fluid (water) from the right side through the parallel cooling channels. The flow is driven along the length L, of the square channel ($w_c = h_c$) with a fixed pressure difference ΔP, in a transverse and counter-direction to the heat flux. An elemental volume shown in Figure 2 consisting of a cooling channel and the surrounding solid was used for analysis because of the assumption of the

symmetrical heat distribution on the left side of the structure. The heat transfer in the elemental volume is a conjugate problem, which combines heat conduction in the solid and the convection in the working fluid.

Design variables

In Figure 2, an elemental volume, v_{el}, constraint is considered to be composed of an elemental cooling channel of hydraulic diameter d_h ($d_h = w_c = h_c$). The surrounding solid of thickness s (spacing between channels) is defined as:

$$w = h \tag{1}$$

The elemental volume is:

$$v_{el} = w^2 L \tag{2}$$

and the width of an elemental volume is:

$$w = d_h + s \tag{3}$$

Therefore, the number of channels in the structure arrangement can be defined as:

$$N = \frac{HW}{(d_h + s)^2} \tag{4}$$

and the void fraction or porosity of the unit structure can be defined as:

$$\phi = \frac{v_c}{v_{el}} = \left(\frac{d_h}{w}\right)^2 \tag{5}$$

The fundamental problem under consideration is the numerical optimisation of the channel hydraulic diameter, d_h, and the channel spacing, s, which corresponds to the minimum resistance of a fixed volume for a specified pressure drop. The optimisation is evaluated from the analysis of the extreme limits of $0 \le d_h \le \infty$ and the extreme limits of $0 \le s \le \infty$. The optimal values of the design variables within the prescribed interval of the extreme limits exhibit the minimum thermal resistance.

The temperature distribution in the elemental volume was determined by solving the equation for the conservation of mass, momentum and energy numerically. A section of the discretised three-dimensional computational domain of the elemental volume is shown in Figure 3. The cooling fluid was water, which was forced through the cooling channels by a specified pressure difference, ΔP, across the axial length of the structure. The fluid is assumed to be in single phase, steady and Newtonian with constant properties. Water as fluid is more promising than air, because air-cooling techniques are not likely to meet the challenge of high heat dissipation in electronic packages [32, 33]. The governing differential equations used for the fluid flow and heat transfer analysis in the elemental volume of the structure are:

$$\nabla \cdot \vec{u} = 0 \tag{6}$$

$$\rho\left(\vec{u} \cdot \nabla \vec{u}\right) = -\nabla P + \mu \nabla^2 \vec{u} \tag{7}$$

$$\rho_f C_{Pf} \left(\vec{u} \cdot \nabla T\right) = k_f \nabla^2 T \tag{8}$$

The energy equation for the solid part of the elemental volume can be written as:

$$k_s \nabla^2 T = 0 \tag{9}$$

The continuity of the heat flux at the interface between the solid and the liquid is given as:

$$k_s \left.\frac{\partial T}{\partial n}\right|_w = k_f \left.\frac{\partial T}{\partial n}\right|_w \tag{10}$$

A no-slip boundary condition is specified for the fluid at the wall of the channel,

$$\vec{u} = 0 \tag{11}$$

At the inlet ($z = L$),

$$u_x = u_y = 0 \tag{12}$$

$$T = T_{in} \tag{13}$$

$$P = \frac{Be\alpha\mu}{L^2} + P_{out} \tag{14}$$

where, the Bejan number 34, 35], *Be,* is the dimensionless pressure difference and given as:

$$Be = \frac{\Delta P L^2}{\mu\alpha_f} \tag{15}$$

and

$$\alpha_f = \frac{k_f}{\rho_f C_{Pf}} \tag{16}$$

At the outlet (z = 0), the pressure is prescribed as zero normal stress

$$P_{out} = 1\ atm \tag{17}$$

At the left side of the wall, the thermal boundary condition that is imposed is assumed to be:

$$q'' = k_s \frac{\partial T}{\partial z} \tag{18}$$

at the solid boundaries, the remaining outside walls and the plane of symmetry were modelled as adiabatic as shown in Figure 2.

$$\nabla T = 0 \tag{19}$$

The measure of performance is the minimum global thermal resistance, which could be expressed in a dimensionless form as:

$$R_{\min} = \frac{k_f \left(T_{\max} - T_{in}\right)_{\min}}{q'' L} \tag{20}$$

and it is a function of the optimised design variables and the peak temperature.

$$R_{\min} = f\left(d_{h_{opt}},\ v_{el_{opt}},\ T_{\max_{\min}}\right) \tag{21}$$

R_{min} is the minimised thermal resistance for the optimised design variables. The inverse of R_{min} is the optimised overall global thermal conductance.

The effect of material properties later be taken into consideration by the ratio of the thermal conductivities

$$k_r = \frac{k_s}{k_f} \qquad 22$$

3. Numerical procedure, grid analysis and code validation

The simulation work began by fixing the length of the channel, prescribed pressure difference, porosity, heat flux and material properties and we kept varying values of hydraulic diameter of the channel in order to identify the best (optimal) internal configuration that minimised the peak temperature. The numerical solution of the continuity, momentum and energy Eqs. (6) - (9) along with the boundary conditions (10) - (19) was obtained by using a three-dimensional commercial package Fluent™ [36], which employs a finite volume method. The details of the method are m explained by Patankar [37]. Fluent™ was coupled with the geometry and mesh generation package Gambit [38] using MATLAB [39] to allow the automation and running of the simulation process. After the simulation had converged, an output file was obtained containing all the necessary simulation data and results for the post-processing and analysis. The computational domain was discretised using hexahedral/wedge elements. A second-order upwind scheme was used to discretise the combined convection and diffusion terms in the momentum and energy equations. The SIMPLE algorithm was then employed to solve the coupled pressure-velocity fields of the transport equations. A flow chart representing the numerical procedure is shown in Figure 4. The solution is assumed to have converged when the normalised residuals of the mass and momentum equations fall below 10^{-6} and while the residual convergence of energy equation was set to less than 10^{-10}. The

number of grid cells used for the simulations varied for different elemental volume and porosities. However, grid independence tests for several mesh refinements were carried out to ensure the accuracy of the numerical results. The convergence criterion for the overall thermal resistance as the quantity monitored was:

$$\gamma = \frac{\left|(T_{\max})_i - (T_{\max})_{i+1}\right|}{\left|(T_{\max})_i\right|} \le 0.01 \tag{23}$$

where i is the mesh iteration index. The mesh was more refined as i increases. The $i-1$ mesh was selected as a converged mesh when the criterion (23) was satisfied.

Table 1 shows the grid independence test performed for the case where d_h = 400 μm and $\phi = 0.2$ for Be = 10^8. Computational cell densities of 3 675, 5952, 11 200 and 20 160 were used for the grid independence test. Almost identical results were predicted when 5 952 and 11 200 cells were used. Therefore, a further increase in the cell density beyond 11 200 has a negligible effect on the results.

Table 1: Grid independence study with $d_h = 400\mu$m and $\phi = 0.2$ for $Be = 10^8$

Number of nodes	Number of cells	$T_{\max}$	$\gamma = \frac{\left\|(T_{\max})_i - (T_{\max})_{i-1}\right\|}{\left\|(T_{\max})_i\right\|}$
5 456	3 675	33.09371	-
8 718	5 952	32.79123	0.009194
15 005	11 200	32.772	0.000587
26 609	20 160	32.67453	0.002983

The validation of the numerical simulation was carried out by comparing the present simulation with that of Kim *et al* [7] for a cylindrical configuration as shown in Figure 5 for

the case where $\phi = 0.1$ and k_r = 10. The curves were found to be similar in trend and the solutions were in good agreement with a deviation of less than 7%.

4. Numerical results

In this section, we present results for the case when the channel hydraulic diameter (or channel width/height) was in the range of 0.1 mm to 1.5 mm and the porosities ranged between $0.1 \leq \phi \leq 0.3$ and a fixed length of L = 10 mm and fixed applied dimensionless pressure differences of $Be = 10^8$. The thermal conductivity of the solid structure (stainless steel) was 16.27 W/m.K; and the heat flux supplied at the left wall was 100 kW/m^2. The thermophysical properties of water [40] used in this study were based on water at 300 K and the inlet water temperature was fixed at this temperature.

Figures 6 and 7 show the existence of an optimum hydraulic diameter and elemental volume size in which the peak temperature is minimised at any point in the channel for the square configuration studied. Figure 6 shows the peak temperature as a function of the channel hydraulic diameter. It shows that there exists an optimal channel hydraulic diameter, which lies in the range $0.01 \leq d_h/L \leq 0.05$ minimising the peak temperature. Also, the elemental volume of the structure has a strong effect on the peak temperature as shown in Figure 7. The minimum peak temperature is achieved when the optimal elemental volume is in the range 0.05 mm^3 $\leq v_{el} \leq$ 8 mm^3. This indicates that the global peak temperature decreases as the design variables (hydraulic diameter and elemental volume) increase or the global peak temperature decreases as the design variables decrease until it gets to the optimal design values. Therefore, any increase or decrease in the design variable beyond the optimal values indicates that the working fluid is not properly engaged in the cooling process, which is detrimental to the global performance of the system. The results show that the optimal

arrangement of the elemental volume for the entire structure at this fixed pressure difference should be very small in order to achieve a better cooling. Figures 6 and 7 also show that porosity has a significant effect on the peak temperature. The best cooling occurs at the highest porosity. That is, as the porosity increases, the peak temperature decreases.

5. Mathematical optimisation and optimisation problem

In this section, we introduce an optimisation algorithm that will search and identify the optimal design variables at which the system will perform at an optimum. A numerical algorithm, Dynamic-Q [41], was employed and incorporated into the finite volume solver and grid (geometry and mesh) generation package by using MATLAB as shown in Figure 4 for more efficient and better accuracy in determining the optimal performance.

The Dynamic-Q is a multidimensional and robust gradient-based optimisation algorithm, which does not require an explicit line search. The technique involves the application of a dynamic trajectory LFOPC optimisation algorithm to successive quadratic approximations of the actual problem [42]. The algorithm is also specifically designed to handle constrained problems where the objective and constraint functions are expensive to evaluate. The details of the Dynamic-Q and applications can be found in open literature [41-47].

5.1 Design variable constraints

The constraint ranges for the optimisation are:

$$0.1 \leq \phi \leq 0.3 \tag{24}$$

$$0 \leq w \leq L \tag{25}$$

$$0 \leq d_h \leq w \tag{26}$$

$$0 \leq s \leq w \tag{27}$$

The design and optimisation technique involves the search for and identification of the best channel layout that minimises the peak temperature, T_{max}, such that the minimum thermal resistance between the fixed volume and the cooling fluid is obtained with the desired objectives function. The hydraulic diameter and the channel spacing and elemental volume of the square configuration were considered as design variables. A number of numerical optimisations and calculations were carried out within the design constraint ranges given in Eqs. (24) – (27) and the results are presented in the succeeding section in order to show the optimal behaviour of the entire system. The optimisation process was repeated for applied dimensionless pressure differences, *Be*, from 10^5 to 10^9.

5.2. Effect of applied pressure difference on optimised geometry and minimised thermal resistance

Figure 8 shows the effect of the minimised thermal resistance as a function of applied dimensionless pressure difference. Minimised thermal resistance decreases as the applied dimensionless pressure difference and porosity increase. Figure 9 shows that the optimal hydraulic diameter decreases as the pressure differences increase and there exists a unique optimal geometry for each of the applied pressure differences. The trend is in agreement with previous work [7, 43].

5.3. *Effect of material properties on optimised geometry minimised thermal resistance*

The effect of material properties on the minimum thermal resistance and optimised internal configuration was also studied. This was best investigated by numerically simulating conjugate heat transfer in an elemental volume for different values of thermal conductivity ratio.

The numerical simulations follow the same procedure already discussed to show the existence of an optimal geometry. We started the simulation by fixing $\phi = 0.2$, $Be = 10^8$ and $k_r = 10$ and $k_r = 100$. We then varied the hydraulic diameter and the elemental volume until we got the minimum peak temperature. Figure 10 shows that optimal geometry exists at different thermal conductivity ratios and minimum peak temperatures are achieved when k_r is high.

We later carried on an optimisation process to determine the best geometry that gives us the lowest thermal resistance temperature by using the optimisation algorithm. We fixed $\phi = 0.2$ and $Be = 10^8$ for all the design constraint ranges and for different values of thermal conductivity ratios ranging from $k_r = 1$ to $k_r = 10^4$. Figures 11 and 12 show the effect of the thermal conductivity ratio on the minimised global thermal resistance and optimised hydraulic diameter at fixed $\phi = 0.2$ and $Be = 10^8$. The minimised thermal resistance decreases as the thermal conductivity ratio increases. This shows that material properties have a strong effect on the thermal resistance. The materials with a high thermal conductivity property reduce the thermal resistance. Figure 12 shows that the thermal conductivity ratio has a significant influence on the optimised hydraulic diameter. As the thermal conductivity ratio increases, the optimal hydraulic diameter increases. However, at higher thermal conductivity ratios (say $Be \geq 4\ 000$), the thermal conductivity has a negligible effect on the minimised thermal resistance and optimised hydraulic diameter.

We repeated the optimisation process for all the design constraint ranges from $k_r = 1$ to 100 for applied dimensionless pressure differences ranging from $Be = 10^5$ to 10^9, and $\phi = 0.1$ to 0.2 to determine the global behaviour of the whole system. Figures 13 to 15 show the effect of the applied dimensionless pressure difference on the minimum thermal resistance and the internal geometry for different values of thermal conductivity ratio and porosity. Figure 13 shows that the minimised thermal resistance decreases as the applied dimensionless

pressure difference, thermal conductivity ratio and porosity increase. Also, Figures 14 and 15 show that there are unique design variables for each applied dimensionless pressure difference, thermal conductivity ratio and porosity.

Figures 16a and 16b show the temperature contours of the elemental volume and of the inner wall of the cooling channel with cooling fluid, respectively. The blue region indicates the region of low temperature and the red region indicates that of high temperature. The arrow indicates the direction of flow.

6. Method of intersection of asymptotes

This section investigated further the numerical solution of the optimisation of flow and heat transfer with the analytical solution. The theoretical analysis for the vascularised configurations followed the application of the intersection of asymptotes method and scale analysis [7, 15, 48-51] to provide the existence of an optimal geometry that minimised the peak temperature and global thermal resistance. The method of intersection of asymptotes outlined by Kim *et al.* [7] was used to determine the optimal geometric shape. The objective was to provide the relationship between the global objective function in terms of global thermal resistance, R, and the varying hydraulic diameter, d_h, in the two extremes at $d_h \to 0$ and $d_h \to \infty$. The optimal geometry value, $d_{h_{opt}}$, that corresponds to, $R_{\min}$, is located approximately where the two asymptotes intercept. The following assumptions were made throughout the analysis: inlet temperature and the pressure difference, ΔP, driving the pump are fixed with a uniform flow distribution in all the channels, laminar flow, constant cross-sectional area of the channels, negligible inlet and exit plenum losses, negligible axial conduction. An elemental volume is treated because of the symmetry of the heat distribution. The analysis of a square volume element is completely analogous to what is presented in Kim

et al. [7], using the same procedure as outlined by Kim *et al.* [7]. We have that the dimensionless thermal resistance, *R*, behaviour in the extreme limit of a small square channel is given as:

$$R = \frac{k_f \left(T_{\max} - T_{\text{in}}\right)}{q'' L} \cong \frac{32}{\phi} \left(\frac{d_h}{L} \right)^{-2} Be^{-1} \tag{28}$$

From Eq. 28, it can be concluded that in the small diameter extreme, R, increases as $d_h \to 0$.

In the opposite extreme limit (large channel), the dimensionless global thermal resistance is defined in terms of dimensionless pressure difference as:

$$R = \frac{k_f \left(T_{\max} - T_{\text{in}}\right)}{q'' L} \cong 0.75 k_r^{-1} \phi^{-1/2} \frac{d_h}{L} \tag{29}$$

From Eq. (29), it can be concluded that in the large channel diameter extreme, R, increases as $d_h \to \infty$.

The geometric optimisation in terms of channel geometry could be achieved by combining Eqs. (28) and (29) using the intersection of asymptotes method as shown in Figure 17. The optimal dimension can generally be approximated for the hydraulic diameter where the two extreme curves intersect. The intersection result is:

$$\frac{d_{h_{opt}}}{L} \approx 3.494 \phi^{-1/6} k_r^{1/3} Be^{-1/3} \tag{30}$$

where $d_{h_{opt}}$ is the optimal hydraulic diameter of the cooling channel.

The optimal spacing s_{opt} between channels follows from Eqs. (3), (5) and (30):

$$\frac{s_{opt}}{L} \approx 3.494 \phi^{-1/6} k_r^{1/3} Be^{-1/3} \left(\phi^{-1/2} - 1 \right) \tag{31}$$

Eqs. (30) and (31) show that in the two extremes, the hydraulic diameter and channel spacing decrease as the pressure difference increases for fixed porosity.

The minimum dimensionless global thermal resistance can be obtained for an elemental volume for the configuration that corresponds to the optimal geometries by substituting Eq. (30) into Eq. (28) as:

$$R_{\min} = \frac{k_f \left(T_{\max} - T_{\text{in}}\right)_{\min}}{q'' L} \cong 2.62 \left(k_r \phi\right)^{-2/3} Be^{-1/3} \tag{32}$$

Equation (32) shows that the minimised global thermal resistance decreases monotonically as, Be , increases for a fixed porosity.

The optimisation results of Eqs. (30) and (32) agreed within a factor of the order of one with th corresponding result of Kim *et al*. [7], because geometrically, the hydraulic diameter of a circular duct and that of a square duct are the same.

7. Correlations of the theoretical method and numerical optimisation

The analytical results of Eqs. (30) to (32) were used to validate the numerical solutions. The numerical and approximate solutions based on scale analysis at optimal geometry dimensions are in good agreement and the solutions have similar trends as shown in Figures 18 to 20.

Figure 18 shows the minimised dimensionless global thermal resistance group as a function of the dimensionless pressure difference at optimised design variables for the configuration. The analytical and the numerical results show that the minimised global thermal resistance group decreases as the dimensionless pressure difference increases. Figures 19 and 20 show the effect of the dimensionless pressure difference on the optimised dimensionless design variable groups. The curves show that the optimised design variables decrease as the applied dimensionless pressure difference and porosity increase. This shows that a unique optimal

design geometry exists for each applied dimensionless pressure difference, thermal conductivity ratio and porosity.

Also the optimised spacing is directly proportional to the optimised hydraulic diameter. This is also due to the fact that the elemental volume is not fixed, but it is allowed to morph for a fixed porosity. In all cases (objective function and design variables), the theoretical and numerical values agree within a factor of the order one for the worst case. These results are also in agreement with past research work [7, 43].

8. Conclusion

This paper studied the numerical and analytical optimisation of geometric structures of square cooling channels of vascularised material with a localised self-cooling property subject to a heat flux on one side in such a way that the peak temperature is minimised at every point in the solid body. The numerical results obtained are in good agreement with results obtained in the approximate solutions based on scale analysis at optimal geometry dimensions. The approximate dimensionless global thermal resistance predicts the trend obtained in the numerical results. This shows that there are unique optimal design variables (geometries) for a given applied dimensionless pressure number for fixed porosity. The use of the optimisation algorithm coupled with the CFD package made the numerical results to be more robust with respect to the selection of optima structure geometries, internal configurations of the flow channels and dimensionless pressure difference.

The results also show that the material property has a significant influence on the performance of the cooling channel. Therefore, when designing the cooling structure of vascularised material, the internal and external geometries of the structure, material properties and pump power requirements are very important parameters to be considered in achieving efficient and optimal designs for the best performance.

Acknowledgements

The funding obtained from the NRF, TESP, Stellenbosch University / University of Pretoria, SANERI/SANEDI, CSIR, EEDSM Hub and NAC is acknowledged and duly appreciated.

References

[1] S.R. White, N.R. Sottos, J. Moore, P. Geubelle, M. Kessler, E. Brown, S. Suresh, S. Viswanathan, Autonomic Healing of Polymer Composites, Nature 409 (2001) 794–797.

[2] A.H. Reis, A.F. Miguel, A. Bejan, Constructal Theory of Particle Agglomeration of Design of Air-cleaning Devices, Journal of Physics D: Applied Physic 39 (2006) 3086–3096.

[3] A. Bejan, S. Lorente, K.-M. Wang, Network of Channels for Self-healing Composite Materials, Journal of Applied Physics 100 (2006) 033528–033528-6.

[4] K.-M. Wang, S. Lorente, A. Bejan, Vascularised Networks with Two Optimised Channels Sizes, Journal Physics D: Applied Physics 39 (2006) 3086–3096.

[5] S.W. Kim, S. Lorente, A. Bejan, Vascularised Materials: Tree-shaped Flow Architectures Matched Canopy to Canopy, Journal of Applied Physics 100 (2006) 063525–063525-8.

[6] S. Lorente, A. Bejan, Heterogeneous Porous Media as Multiscale Structures for Maximum Flow Access, Journal of Applied Physics, 100 (2006) 114909–114909-8.

[7] S.W. Kim, S. Lorente, A. Bejan, Vascularised Materials with Heating from One Side and Coolant Forced from the Other Side, International Journal of Heat and Mass Transfer 50 (2007) 3498–3506.

[8] A. Bejan, Advanced Engineering Thermodynamics, 2nd ed., Wiley, New York, 1997.

[9] A. Bejan, Shape and Structure from Engineering to Nature, Cambridge University Press, Cambridge, UK, 2000.

[10] A. Bejan, E. Sciubba, The Optimal Spacing of Parallel Plates Cooled By Forced Convection, International Journal of Heat and Mass Transfer 35 (1992) 3259–3264.

[11] A. Bejan, S. Lorente, Constructal Theory of Generation of Configuration in Nature and Engineering, Journal of Applied. Physics 100 (2006) 041301.

[12] A. Bejan, S. Lorente, Design with Constructal Theory, Hoboken Wiley, 2008.

[13] A.H. Reis, Constructal Theory: From Engineering to Physics and How Flow Systems Develop Shape and Structure, Applied Mechanics Reviews 59 (2006) 269–282.

[14] Y. Fan, L. Luo, Recent Applications of Advances In Microchannel Heat Exchangers And Multi-Scale Design Optimisation, Heat Transfer Engineering 29 (2008) 461–474.

[15] T. Bello-Ochende, L. Liebenberg, J.P. Meyer, Constructal Cooling Channels for Micro-channel Heat Sinks, International Journal of Heat and Mass Transfer 50 (2007) 4141–4150.

[16] L.A.O. Rocha, E. Lorenzini, C. Biserni, and Y. Cho, Constructal design of a cavity cooled by convection, International Journal of Design and Nature and Ecodynamics, 5 (2010) 212–220.

[17] C. Biserni, L.A.O. Rocha G. Stanescu, and E. Lorenzini, Constructal H-shaped cavities according to Bejan's theory International Journal of Heat and Mass Transfer 50 (2007) 2132–2138.

[18] G. Lorenzini, C. Biserni, and L.A.O. Rocha, Geometric Optimization of Isothermal Cavities according to Bejan's theory. International Journal of Heat Mass Transfer, 54 (2011) 3868–3873.

[19] K-H. Cho, J. Lee, H.S. Ahn, A. Bejan, and M.H. Kim, Fluid Flow and Heat Transfer in Vascularised Cooling Plates, International Journal of Heat and Mass Transfer 53 (2010) 3607–3614.

[20] S. Lorente, and A. Bejan, Svelteness, Freedom to Morph, and Constructal Multi-Scale Flow Structures, International Journal of Thermal Sciences 44 (2005) 1123–1130.

[21] K-M Wang, S Lorente and A Bejan, Vascularisation With Grids of Channels: Multiple Scales, Loops and Body Shapes, Journal of Physics D, Applied Physics 40 (2007) 4740–4749.

[22] S. Kim, S. Lorente and A. Bejan, Dendritic Vascularisation for Countering Intense Heating From The Side, International Journal of Heat and Mass Transfer 51 (2008) 5877–5886

[23] S. Kim, S. Lorente, A. Bejan, W. Miller, and J. Morse, The Emergence of Vascular Design in Three Dimensions , Journal of Applied Physics 103 (2008) 123511-1 123511-8.

[24] K-M. Wang, S. Lorente, A. Bejan, Vascular Materials Cooled With Grids and Radial Channels. International Journal of Heat and Mass Transfer 52, (2009) 1230–1239.

[25] E. Cetkin, S. Lorente, and A. Bejan, 2010, Natural Constructal Emergence of Vascular Design With Turbulent Flow, Journal of Applied Physics., 107 (2010) 4901-1–114901-9

[26] A. V. Azad and M. Amidpour, Economic Optimization of Shell and Tube Heat Exchanger based on Constructal Theory, Energy 36 (2011) 1087 – 1096.

[27] A. Beyene, and J. Peffley, Constructal Theory, Adaptive Motion, and Their Theoretical Application to Low-speed Turbine Design, Journal of Energy Engineering -ASCE, 135 (2009) 112-118.

[28] Y. Kim, S. Lorente, and A. Bejan, Constructal Multi-tube Configuration for Natural and Forced convection in cross-flow International Journal of Heat Mass Transfer, 53 (2010) 5121-5128.

[29] Y. Kim, S. Lorente, and A. Bejan, 2011, Steam Generator Structure: Continuous Model and Constructal Design, International Journal of Energy Research., 35 (2011) 336-345.

[30] J.P., Meyer, Constructal Law in Technology, Thermofluid and Energy Systems, and in Design Education, Physics of life Reviews 8 (2011) 247–248.

[31] A. Bejan, S. Lorente, The Constructal Law and The Evolution of Design in Nature. Physics of Life Reviews 8 (2011) 209–240 .

[32] R.C. Chu, Thermal Management Roadmap Cooling Electronic Products from Hand Held Device To Supercomputers Proc. MIT Rohsenow Symposium Cambridge, MA. 2002.

[33] SEMATECH The National Technology Roadmap for Semiconductors: Technology Needs SEMATECH, Austin TX, 1997.

[34] S. Bhattacharjee, W.L. Grosshandler, The Formation of Wall Jet Near A High Temperature Wall Under Microgravity Environment, ASME HTD 96 (1988) 711–716.

[35] S. Petrescu, Comments On The Optimal Spacing of Parallel Plates Cooled by Forced Convection, International Journal of Heat and Mass Transfer 37 (1994) 1283.

[36] Fluent Inc., Fluent Version 6 Manuals, Centerra Resource Park, 10 Cavendish Court, Lebanon, New Hampshire, USA, 2001 (www.fluent.com).

[37] S.V. Patankar, Numerical Heat Transfer and Fluid Flow, Hemisphere, New York, 1980.

[38] Fluent Inc., Gambit Version 6 Manuals, Centerra Resource Park, 10 Cavendish Court, Lebanon, New Hampshire, USA, 2001 (www.fluent.com).

[39] The MathWorks, Inc., MATLAB & Simulink Release Notes for R2008a, 3 Apple Hill Drive, Natick, MA, 2008 (www.mathworks.com).

[40] F.M. White, Viscous Fluid Flow, 2nd Edition, McGraw-Hill International Editions, Singapore, 1991.

[41] J.A. Snyman, A.M. Hay, The DYNAMIC-Q Optimization Method: An alternative to SQP? Computer and Mathematics with Applications 44 (2002) 1589–1598.

[42] J.A. Snyman, N. Stander, W.J. Roux, dynamic penalty function method for the solution of structural optimization problems, Appl. Math. Model. 18 (1994) 453–460.

[43] O.T. Olakoyejo, T. Bello-Ochende, J.P. Meyer, Geometric Optimisation of Forced Convection in a Vascularised Material, Proc. of the 8th International Conf. on Heat Transfer, Fluid Mechanics and Thermodynamics, Pointe Aux Piments, Mauritius, pp. 38 – 43, 2011.

[44] J.A. Visser, D.J. de Kock, Optimization Of Heat Sink Mass Using The DYNAMIC-Q Numerical Optimization Method, Communications in Numerical Methods in Engineering 18 (2002) 721–727.

[45] T. Bello-Ochende, J.P. Meyer, F.U. Ighalo, Combined Numerical Optimization and Constructal Theory for the Design of Microchannel Heat Sinks, Numerical Heat Transfer, Part A, 58 (2010) 882–899.

[46] R.M. Morris, J.A. Synyman, J. P. Meyer, Jets in Crossflow Mixing Analysis Using Computational Fluid Dynamics and Mathematical Optimization, AIAA Journal of Propulsion and Power, 23 (2007) 618-628.

[47] O.S. Motsamai, J. A. Synyman, J. P. Meyer, Optimisation of Gas Turbine Combustor Mixing For Improved Exit Temperature Profile, Heat Transfer Engineering, 31 (2010) 402-418.

[48] T. Bello-Ochende, J.P. Meyer, J. Dirker, Three-dimensional multi-scale plate assembly for

maximum heat transfer rate density, International Journal of Heat and Mass Transfer, 53 (2010) 586–593.

[49] A. Bejan, Convection Heat Transfer, third ed., Wiley, Hoboken, 2004.

[50] T. Bello-Ochende, J.P. Meyer, A. Bejan, Constructal multi-scale pin fins, International Journal of Heat and Mass Transfer 53 (2010) 2773–2779.

List of Figures

Figure 1 Three-dimensional parallel square channels across a slab with heat flux from one side and forced flow from the opposite side

Figure 2 The boundary conditions of the three-dimensional computational domain of the elemental volume

Figure 3 A section of the discretised 3-D computational domain of the elemental solid-fluid volume considered for the simulation

Figure 4 Flow chart of numerical simulation

Figure 5 Comparison of the results of the present numerical study with those of Kim *et al.* [7] for $\phi = 0.1$ and $k_r = 10$]

Figure 6 Effect of optimised dimensionless hydraulic diameter d_h on the peak temperature at $Be = 10^8$

Figure 7 Effect of optimised elemental volume on the peak temperature at Be = 10^8

Figure 8 Effect of dimensionless pressure difference on the dimensionless global thermal resistance

Figure 9 The effect of dimensionless pressure difference on the optimised hydraulic diameter

Figure 10 Effect of thermal conductivity ratio, k_r, on the peak temperature at a Bejan number of 10^8 and porosity of 0.2

Figure 11 Effect of thermal conductivity ratio, k_r, on the minimised dimensionless global thermal resistance at Be = 10^8 and porosity of 0.2

Figure 12 Effect of thermal conductivity ratio k_r on the optimised hydraudric diameter at Be = 10^8 and porosity of 0.2

Figure 13 Effect of thermal conductivity ratio k_r, porosity, and dimensionless pressure difference on the minimised dimensionless global thermal resistance

Figure 14 Effect of thermal conductivity ratio k_r, porosity, and dimensionless pressure difference on the optimised hydraulic diameter

Figure 15 Effect of thermal conductivity ratio k_r, porosity, and dimensionless pressure difference on the optimised spacing

Figure 16 Temperature distributions on (a) the elemental volume and (b) the cooling fluid and the inner wall

Figure 17 Method of intersection of asymptotes: global thermal resistance

Figure 18 Correlation of numerical and analytical solutions for the minimised global thermal resistance

Figure 19 Correlation of numerical and analytical solutions for the optimised hydraulic diameter

Figure 20 Correlation of numerical and analytical solutions for the optimised spacing

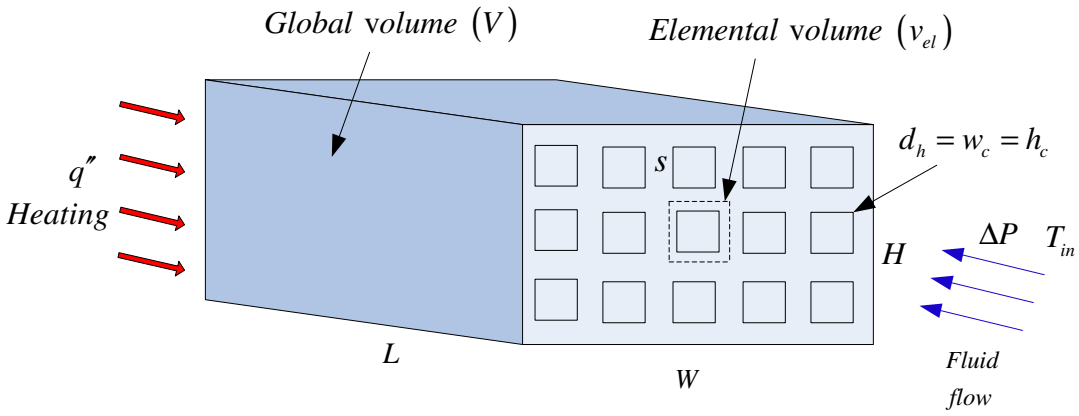
Global volume (V)
Elemental volume (v_{el})
q''
Heating
s
$d_h = w_c = h_c$
H
ΔP
T_{in}
L
W
Fluid
flow

Figure 1

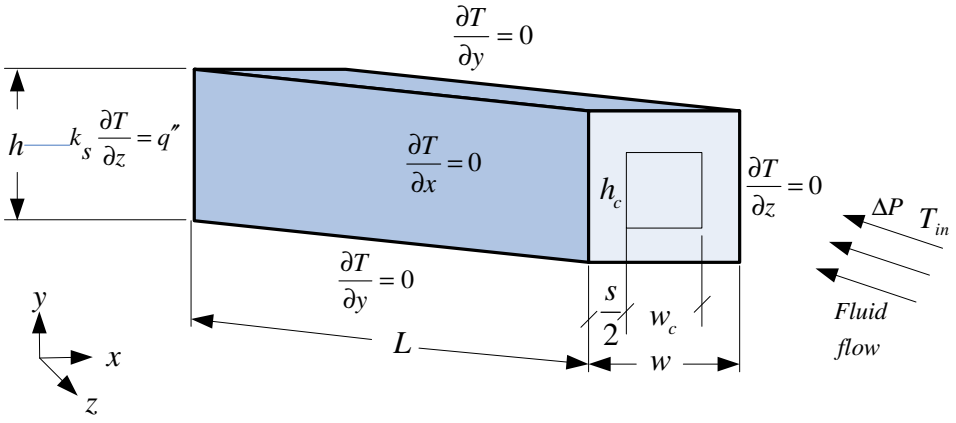
$\frac{\partial T}{\partial y} = 0$
h
$k_s \frac{\partial T}{\partial z} = q''$
$\frac{\partial T}{\partial x} = 0$
h_c
$\frac{\partial T}{\partial z} = 0$
ΔP
T_{in}
$\frac{\partial T}{\partial y} = 0$
$\frac{s}{2}$
w_c
L
w
Fluid flow
y
x
z

Figure 2

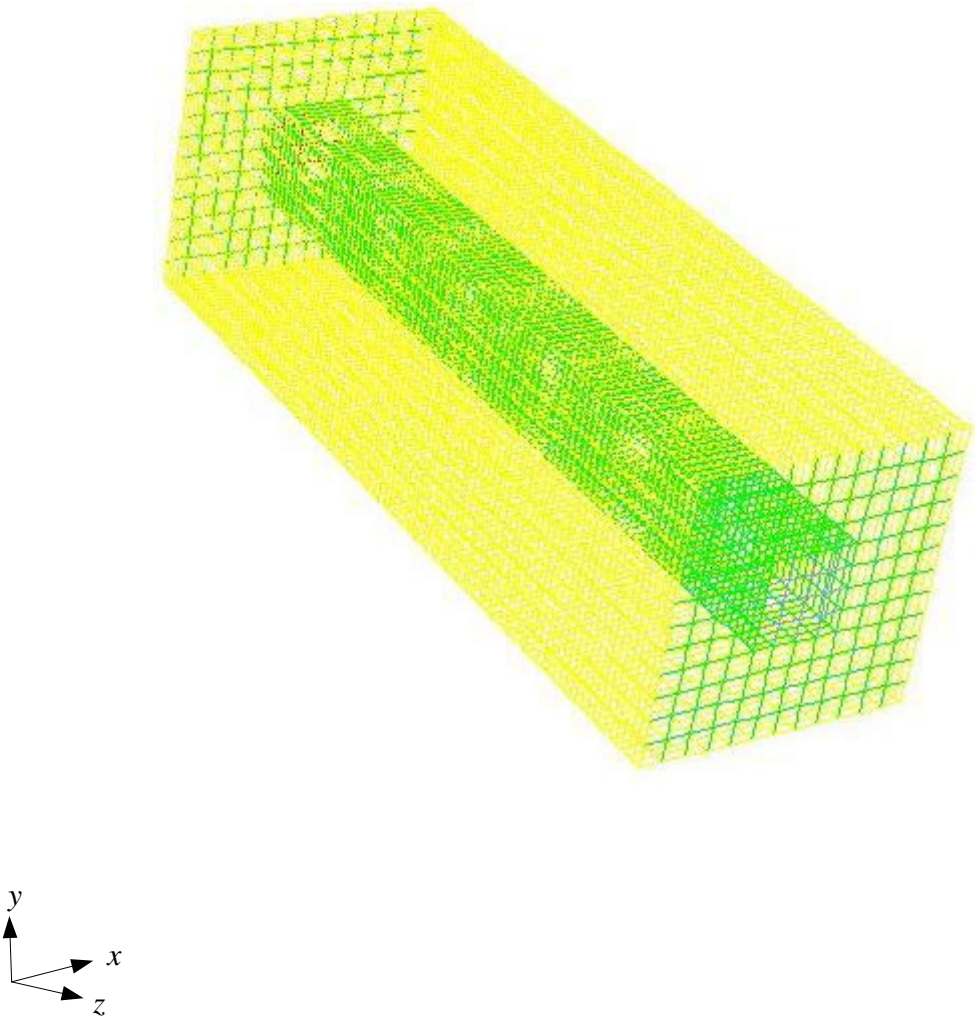

Figure 3

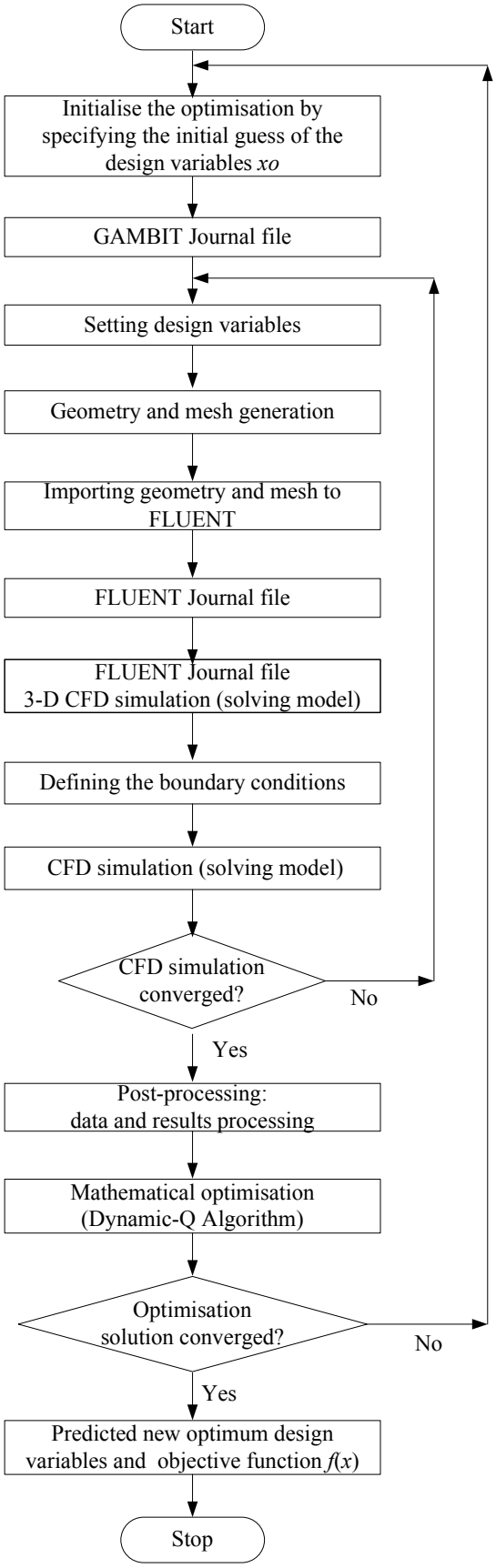
Start
Initialise the optimisation by specifying the initial guess of the design variables xo
GAMBIT Journal file
Setting design variables
Geometry and mesh generation
Importing geometry and mesh to FLUENT
FLUENT Journal file
FLUENT Journal file
3-D CFD simulation (solving model)
Defining the boundary conditions
CFD simulation (solving model)
CFD simulation converged?
No
Yes
Post-processing: data and results processing
Mathematical optimisation (Dynamic-Q Algorithm)
Optimisation solution converged?
No
Yes
Predicted new optimum design variables and objective function f(x)
Stop

Figure 4

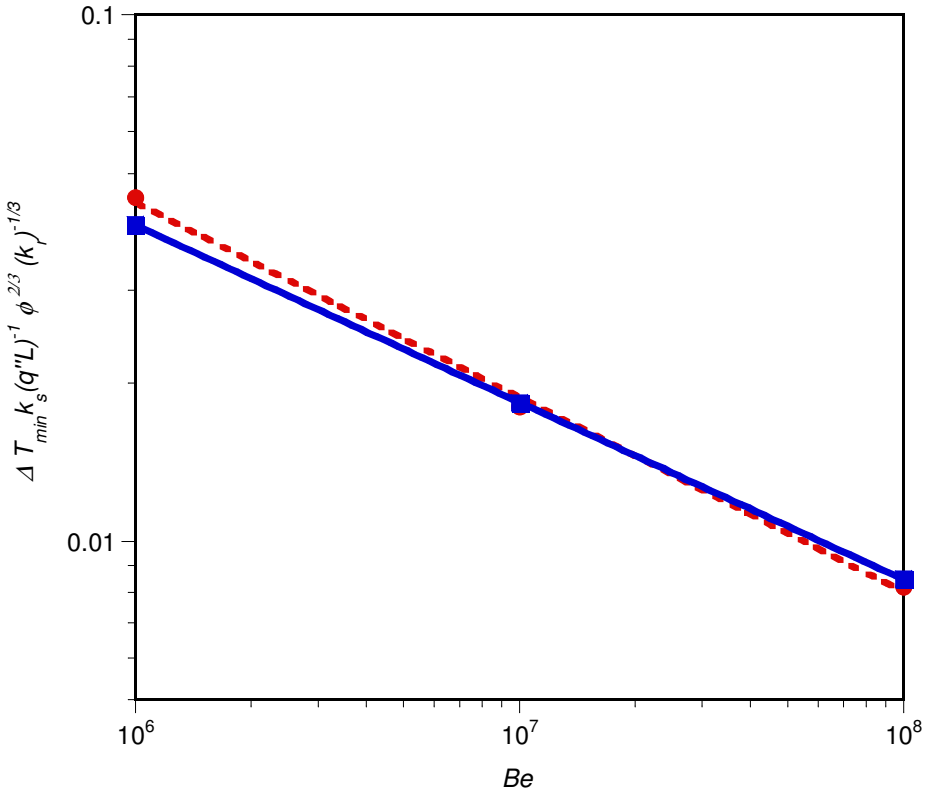

Figure 5

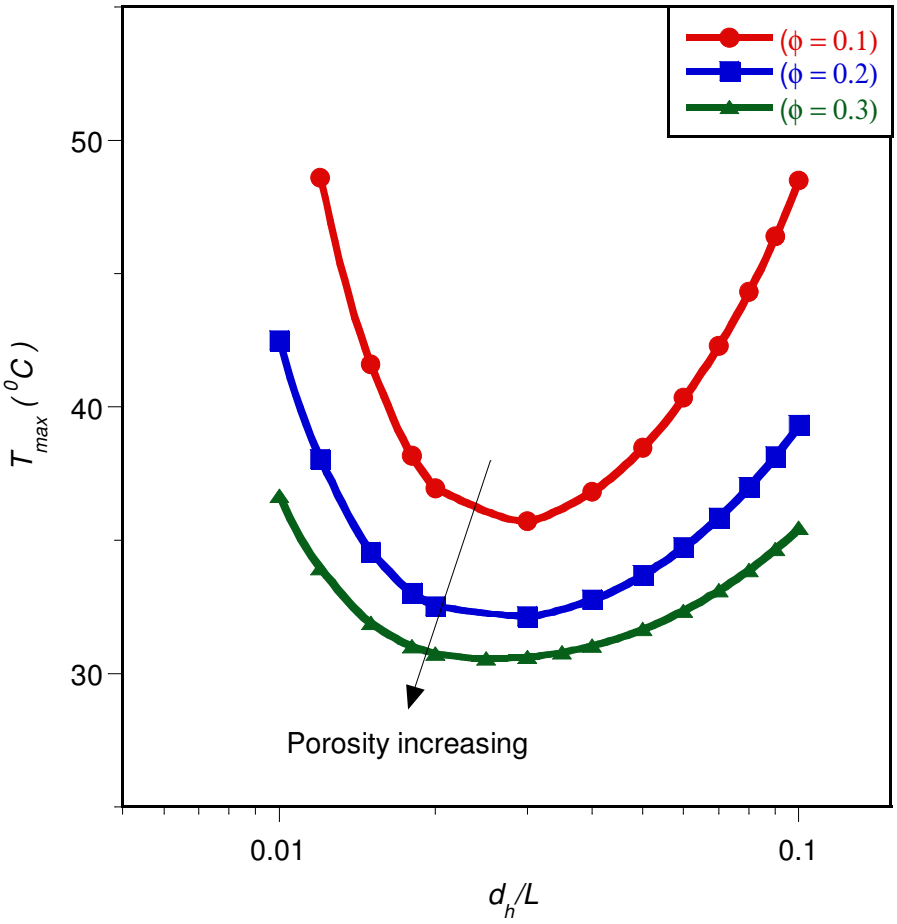

Figure 6

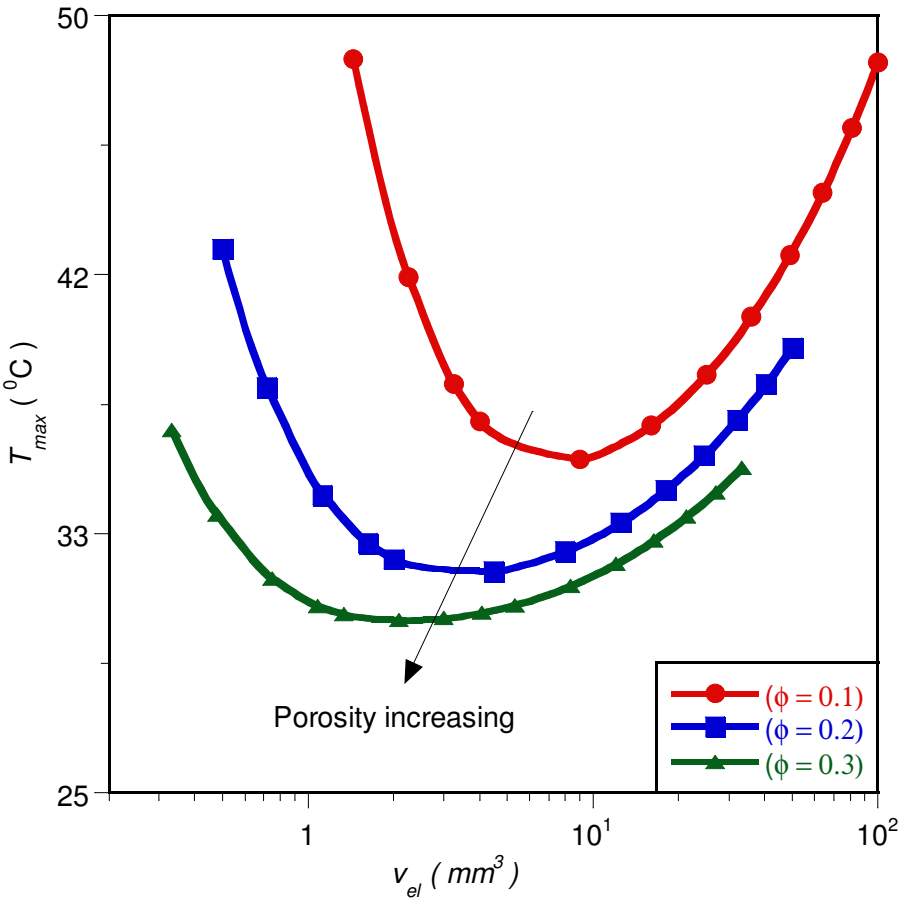
50
42
33
25
1
10^1
10^2
T_max (^0C)
v_el (mm^3)
Porosity increasing
(ϕ = 0.1)
(ϕ = 0.2)
(ϕ = 0.3)

Figure 7

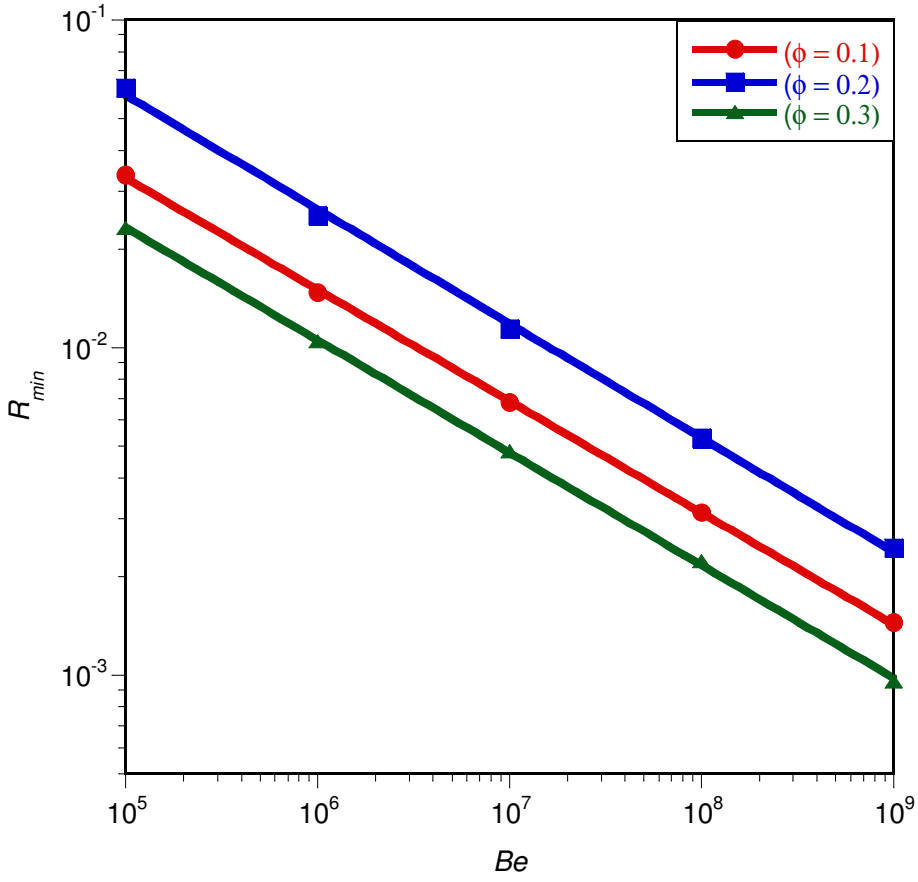

Figure 8

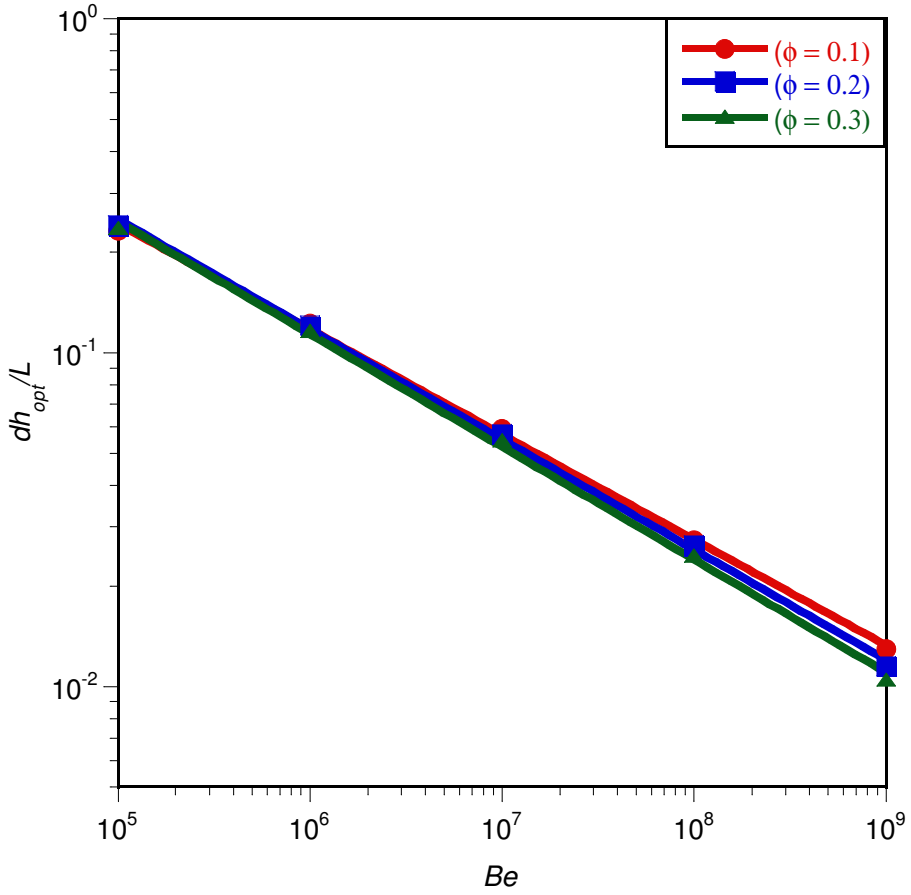

Figure 9

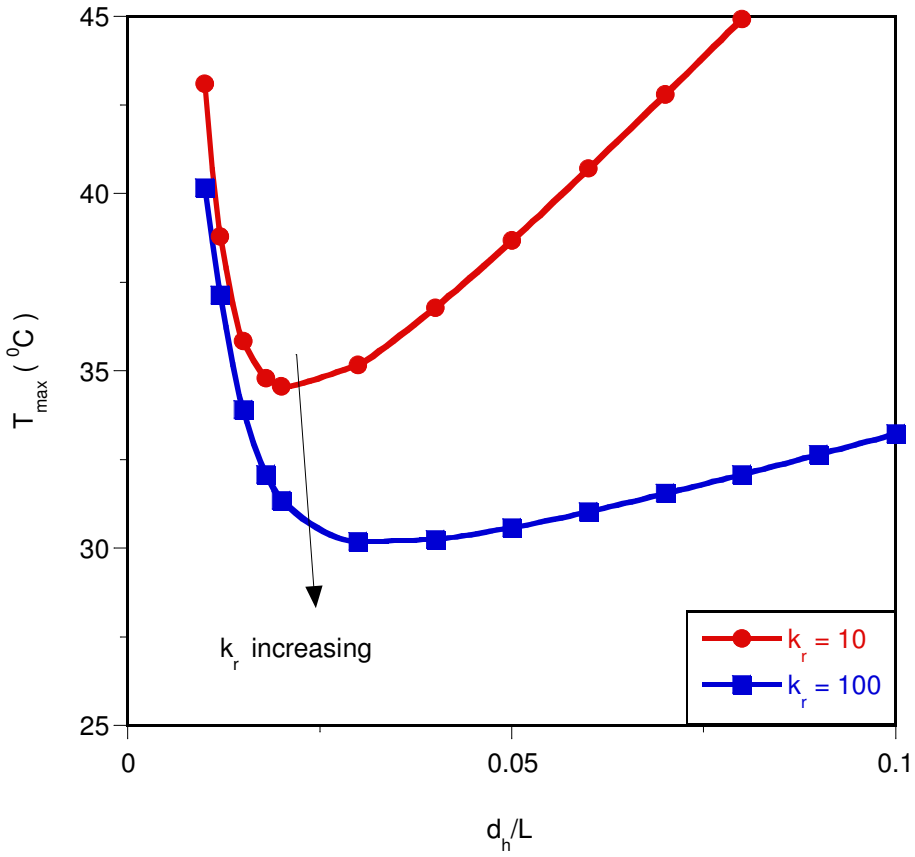

Figure 10

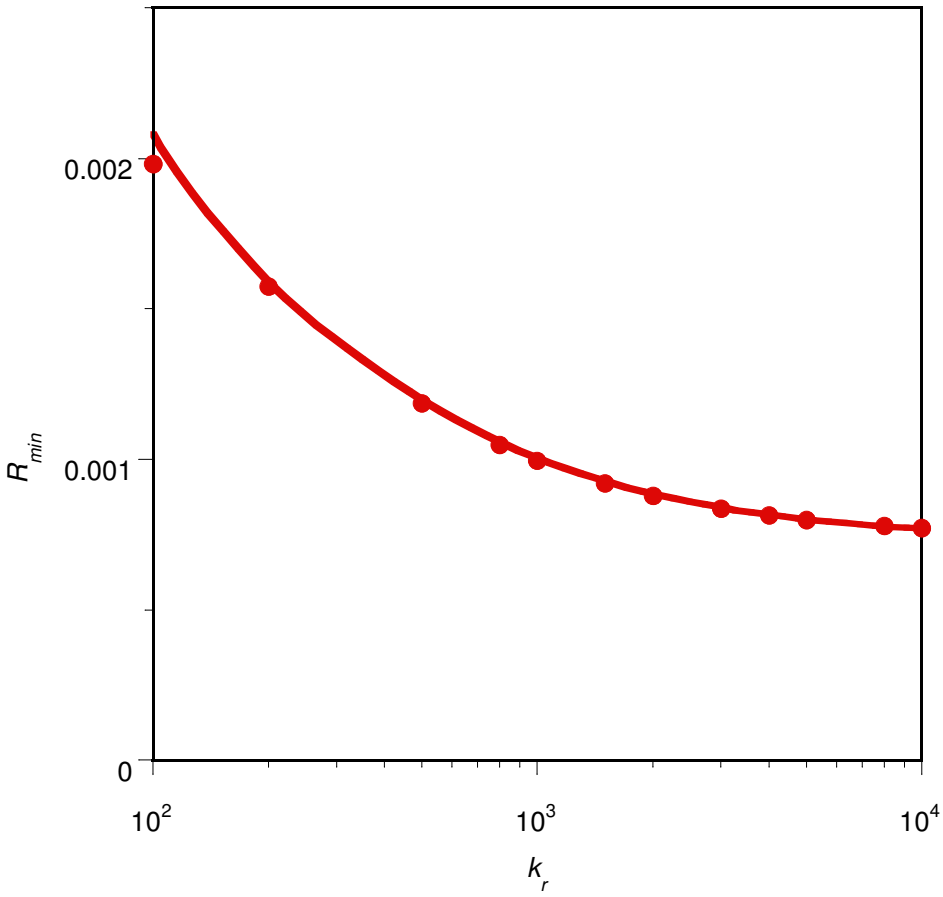

Figure 11

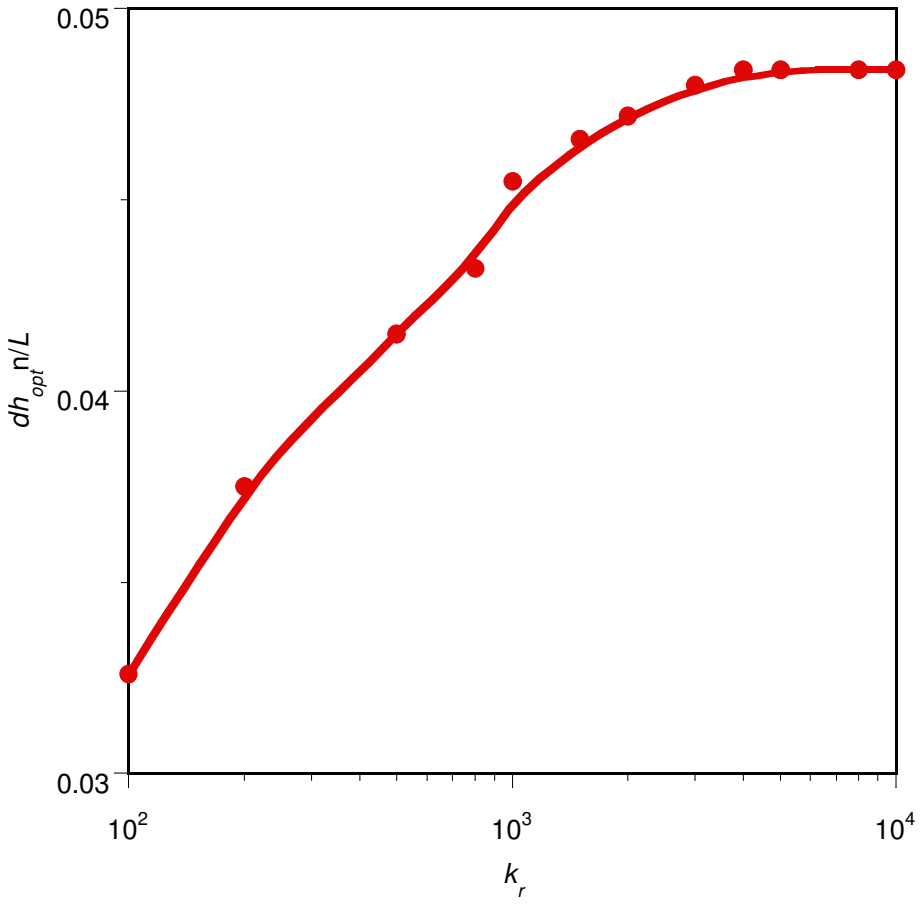

Figure 12

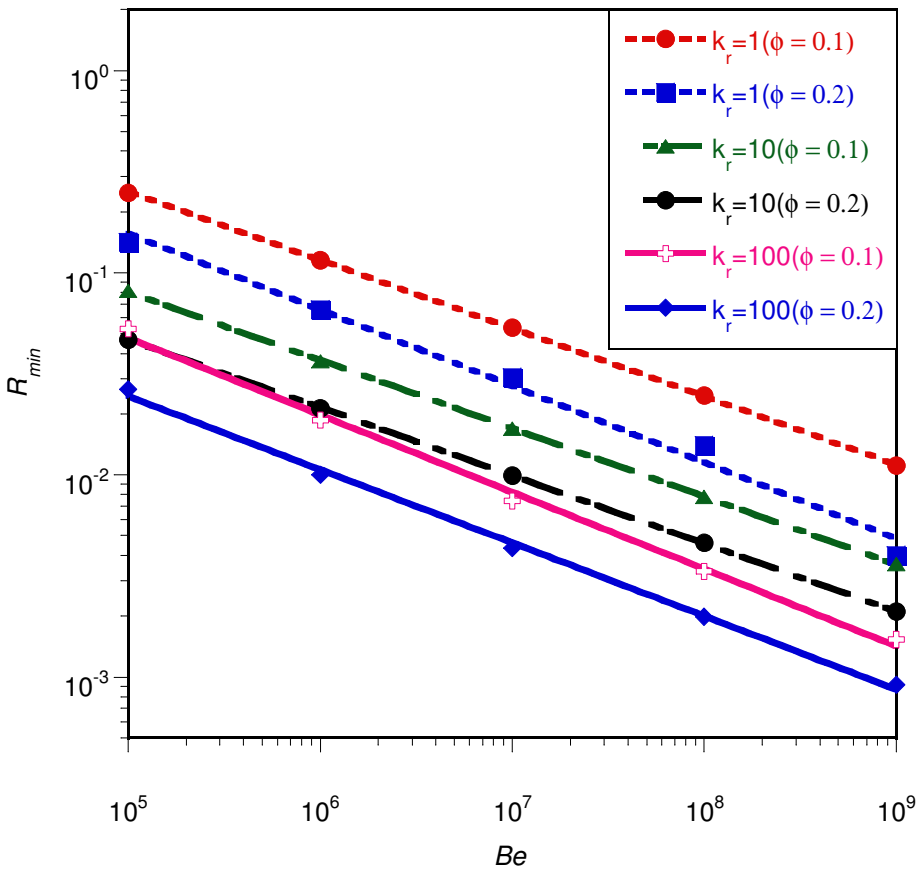
k_r=1(ϕ = 0.1)
k_r=1(ϕ = 0.2)
k_r=10(ϕ = 0.1)
k_r=10(ϕ = 0.2)
k_r=100(ϕ = 0.1)
k_r=100(ϕ = 0.2)
10^0
10^-1
10^-2
10^-3
R_min
10^5
10^6
10^7
10^8
10^9
Be

Figure 13

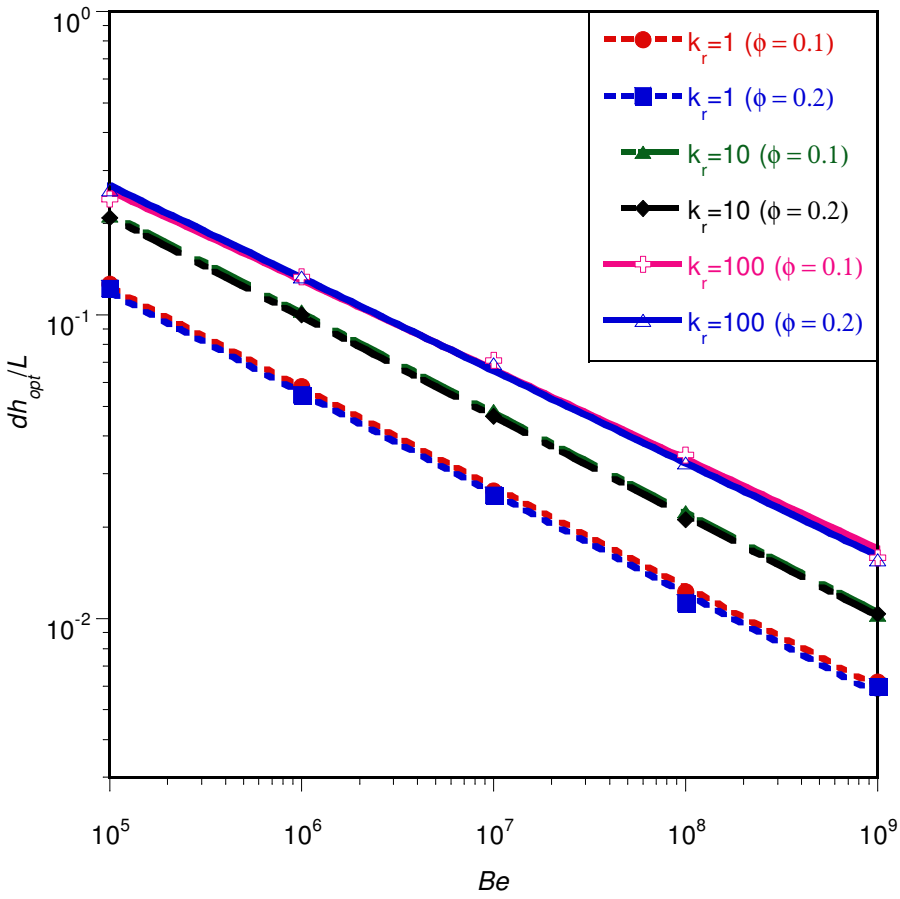
10^0
10^{-1}
10^{-2}
dh_{opt}/L
10^5
10^6
10^7
10^8
10^9
Be
k_r=1 (ϕ = 0.1)
k_r=1 (ϕ = 0.2)
k_r=10 (ϕ = 0.1)
k_r=10 (ϕ = 0.2)
k_r=100 (ϕ = 0.1)
k_r=100 (ϕ = 0.2)

Figure 14

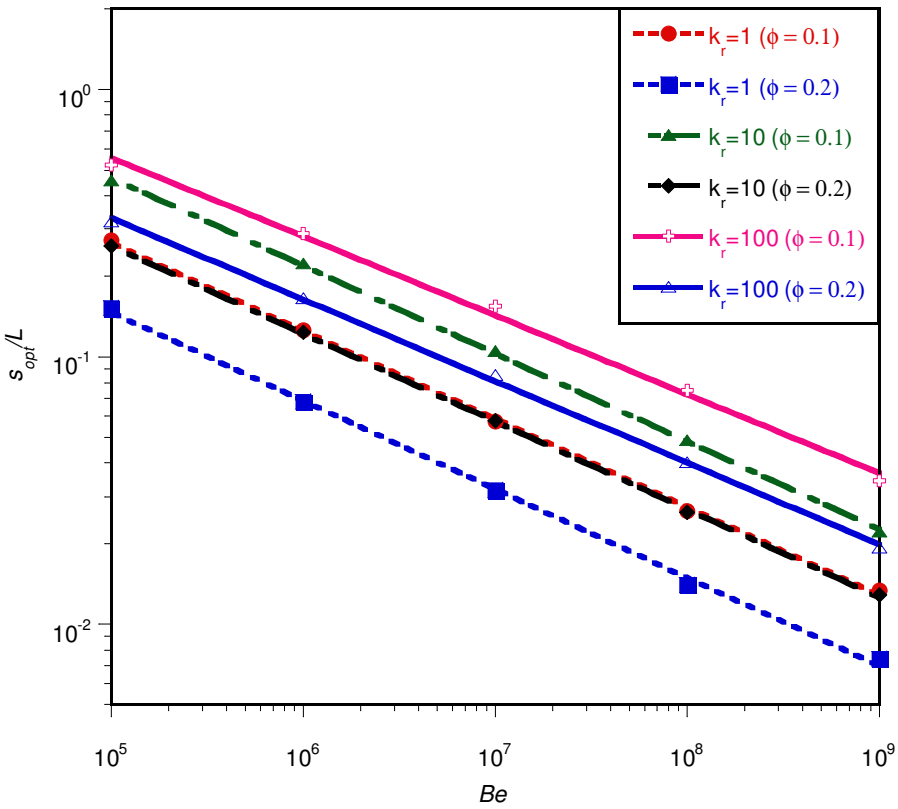
k_r=1 (ϕ = 0.1)
k_r=1 (ϕ = 0.2)
k_r=10 (ϕ = 0.1)
k_r=10 (ϕ = 0.2)
k_r=100 (ϕ = 0.1)
k_r=100 (ϕ = 0.2)
10^0
10^-1
10^-2
s_opt/L
10^5
10^6
10^7
10^8
10^9
Be

Figure 15

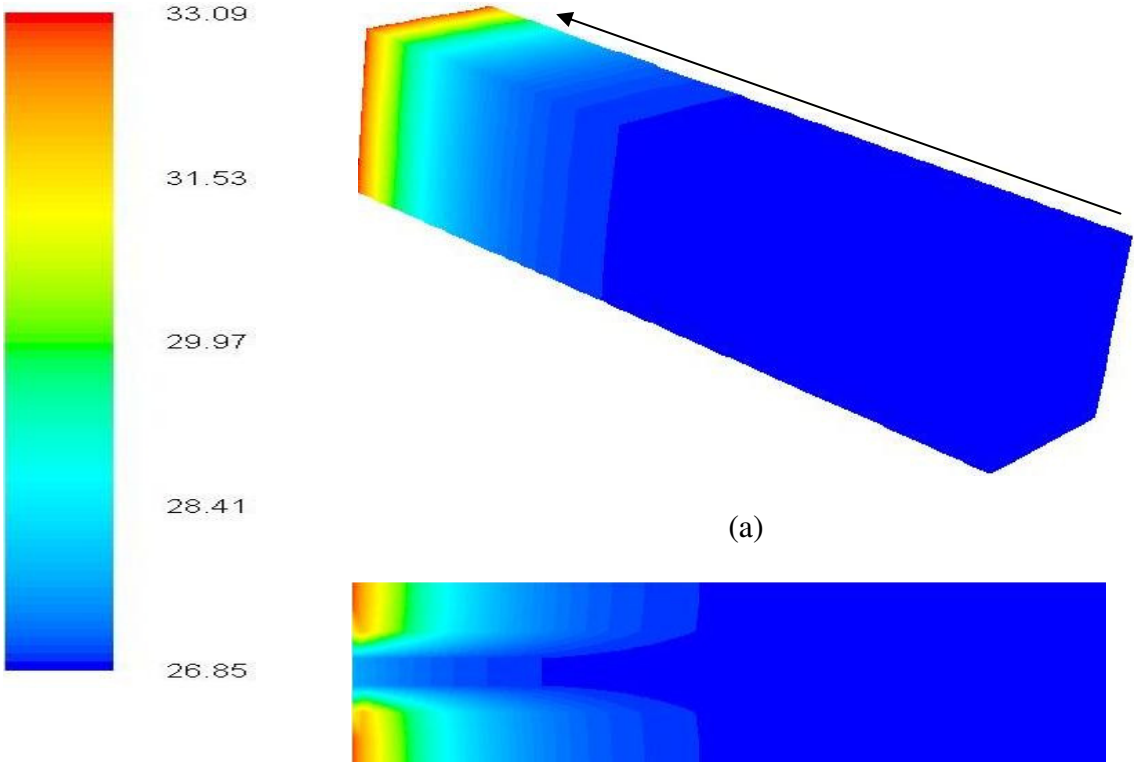

(a)

(b)

Figure 16

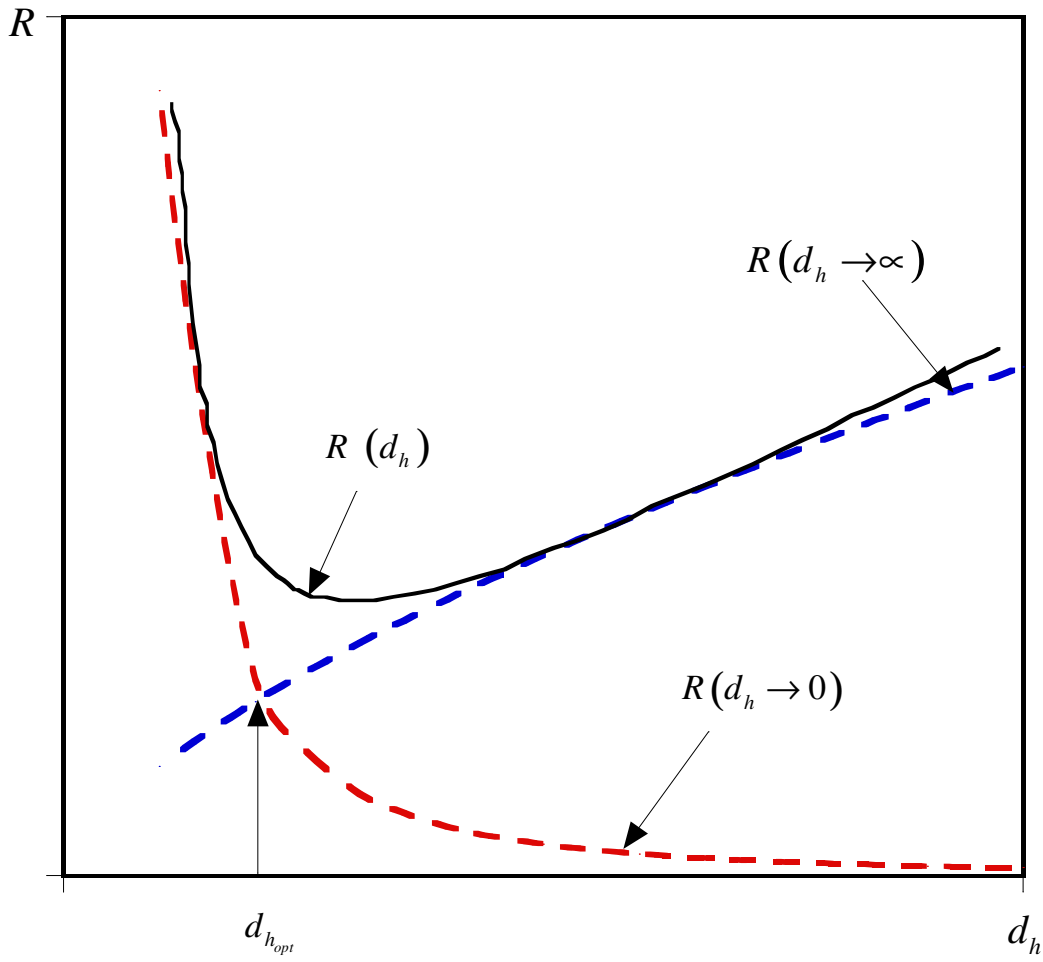

Figure 17

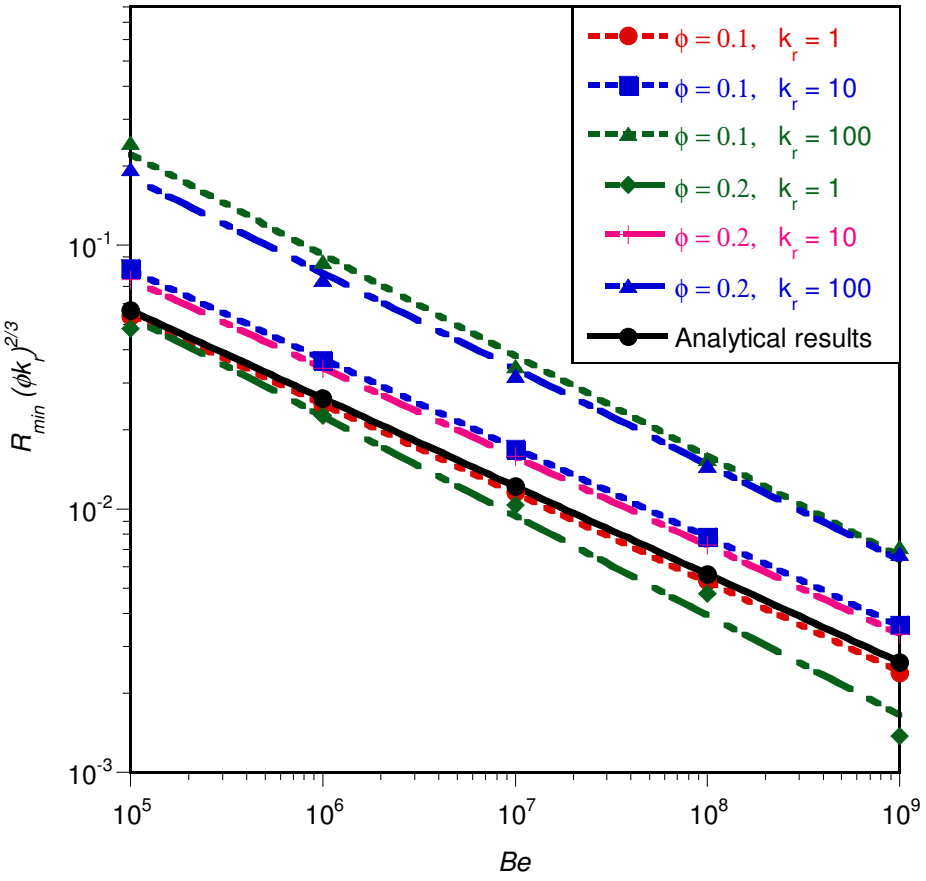
ϕ = 0.1, k_r = 1
ϕ = 0.1, k_r = 10
ϕ = 0.1, k_r = 100
ϕ = 0.2, k_r = 1
ϕ = 0.2, k_r = 10
ϕ = 0.2, k_r = 100
Analytical results
R_min (ϕk_r)^2/3
Be
10^-1
10^-2
10^-3
10^5
10^6
10^7
10^8
10^9

Figure 18

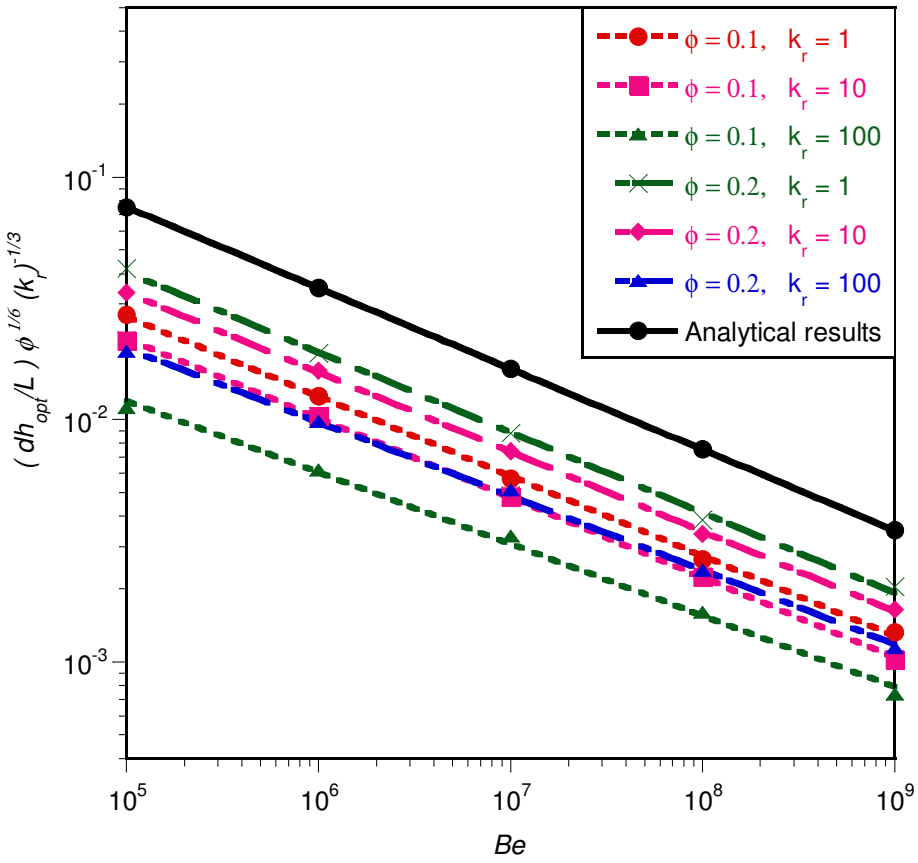
ϕ = 0.1, k_r = 1
ϕ = 0.1, k_r = 10
ϕ = 0.1, k_r = 100
ϕ = 0.2, k_r = 1
ϕ = 0.2, k_r = 10
ϕ = 0.2, k_r = 100
Analytical results
(dh_opt/L) ϕ^1/6 (k_r)^-1/3
10^-1
10^-2
10^-3
10^5
10^6
10^7
10^8
10^9
Be

Figure 19

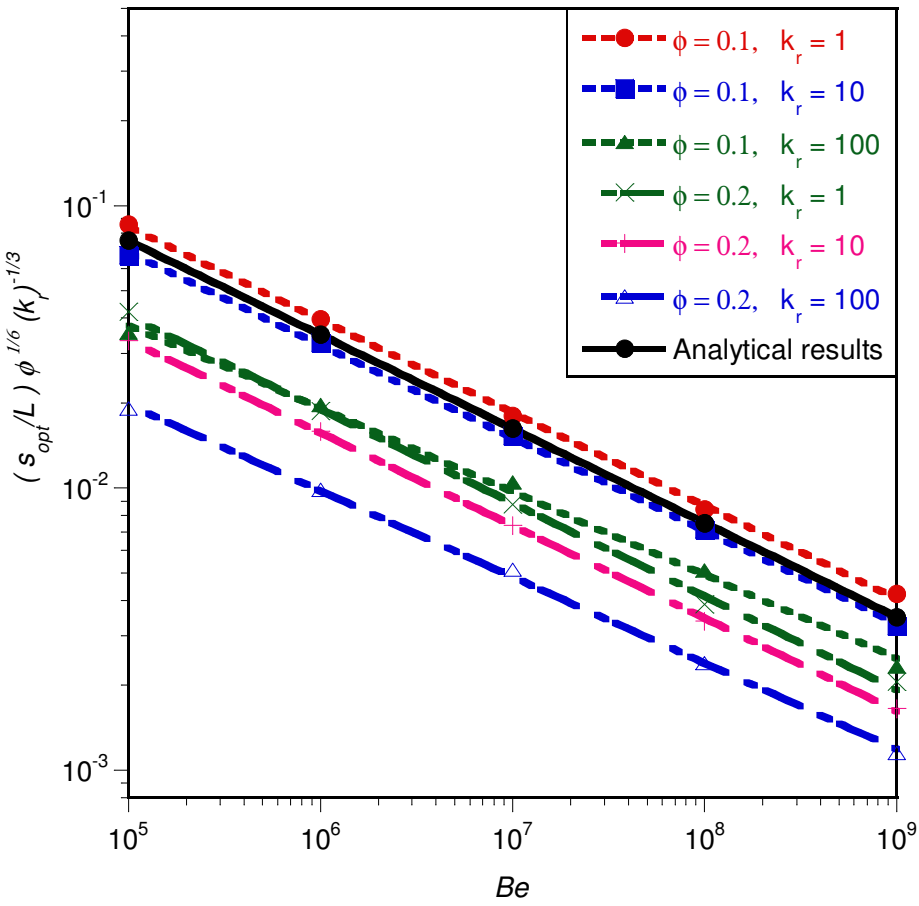
ϕ = 0.1, k_r = 1
ϕ = 0.1, k_r = 10
ϕ = 0.1, k_r = 100
ϕ = 0.2, k_r = 1
ϕ = 0.2, k_r = 10
ϕ = 0.2, k_r = 100
Analytical results
10^-1
10^-2
10^-3
10^5
10^6
10^7
10^8
10^9
Be
(s_opt/L) ϕ^1/6 (k_r)^-1/3

Figure 20